ACS APPLIED MATERIALS & INTERFACES

Research Article

www.acsami.org

Eliminating Heat Injury of Zeolite in Hemostasis via Thermal Conductivity of Graphene Sponge

Yuping Liang,[†] Congcong Xu,[†] Fang Liu,[‡] Shiyu Du,[‡] Guofeng Li,[*,†,§] and Xing Wang[*,†,§]

[†]Beijing Laboratory of Biomedical Materials, Beijing University of Chemical Technology, Beijing 100029, P. R. China

[‡]Department of Gastroenterology, China-Japan Friendship Hospital, Beijing 100029, P. R. China

[§]Key Laboratory of Biomedical Materials of Natural Macromolecules, Beijing University of Chemical Technology, Ministry of Education, Beijing 100029, P. R. China

Supporting Information

ABSTRACT: Thermal release of zeolite is conducive in hemostasis, but losing control will cause serious burns. How to balance the advantages and disadvantages is a challenge. Herein, a zeolite/cross-linked graphene sponge (Z-CGS) was design to break through this challenge. The CGS managed the heat release of zeolite by thermal conduction of graphene. Infrared thermal imager demonstrated the mild exothermic process and good thermal conductivity of the optimized Z-CGS. It controlled wound temperature below 42 °C effectively, as compared to 70 °C of naked zeolite. Blood clotting index further confirmed the contribution of thermal stimulation in Z-CGS. On the synergy of thermal and charge stimulations of zeolite, as well as physical adsorption of CGS, Z-CGS achieved outstanding hemostatic performance. Bleeding was stopped within 69 s in rat artery injury model, faster than that of the Quikclot Combat Gauze. Additionally, cytotoxicity assay and pathological analysis highlighted its biocompatibility. Z-CGS, therefore, was an outstanding composite of combining advantages of zeolite and graphene, while getting rid of the shortcomings of the basic unit. The thermal conductibility of graphene renews an avenue for the safe and highly efficient use of zeolite in hemostasis.

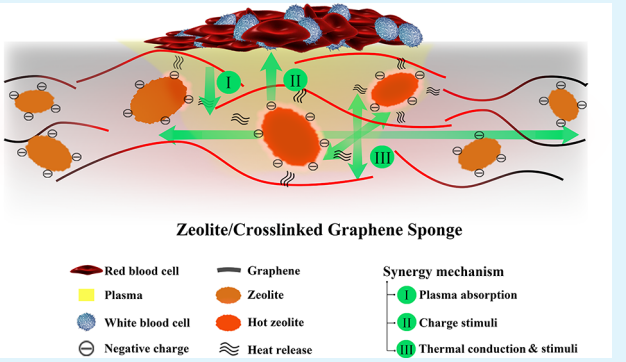

KEYWORDS: *zeolite, graphene, composite, hemostasis, thermal conduction*

1. INTRODUCTION

Using safe and efficient hemostats to stop bleeding is critical for saving lives by avoiding serious complications such as hemorrhagic shock, microbial infection, and multiple organ failures.[1−5] Zeolite is the most classic hemostat, which was widely used since FDA approval in 2002.[6−9] However, the use of naked zeolite would result in severe thermal injury and necrosis of surrounding tissues because its exothermic reaction raises the wound temperature as high as 65 °C.[9−14] To eliminate the exothermic reactions of zeolite, Z-Medica developed a prehydrated zeolite formulation, ACS+, that produces less exothermic reaction. Its hemostatic performance, however, decreased with the weakened absorbability.[11,15,16] Additionally, Ahuja at el replaced calcium ions in zeolite with other positively charged ions to reduce exothermic reaction and attenuate heat-induced tissue damage. However, the wound tissue still heated to 50 °C during hemostasis.[11] Up to now, it has still been a challenge to achieve a win−win situation in both hemostatic performance and heat release in zeolite. Importantly, previous studies revealed that proper heating can accelerate coagulation by directly enhancing platelet function.[17] When platelets are exposed to the stress of heat, they show morphological changes and become more responsive to stimulation.[18−20] Therefore, a better approach is being sought for managing the exothermic reaction of zeolite, in which thermal injury of zeolite could be prevented and the thermal coagulated stimulation could be excited.

Composite strategy is a cradle for developing functional materials. Recently, our group developed a cross-linked graphene sponge (CGS) that acted as a platform for hemostat developing. The CGS possesses many remarkable properties, such as facile preparation, being lightweight, fast liquid adsorption capacity, and good biocompatibility.[21,22] Importantly, the CGS can tightly anchor different clays by rich interactions. The fixed clay inside two-dimensional graphene sheets avoids direct contact with the wound, which eliminates its side effects while maintaining the stimulation for blood clotting. The obtained graphene/clay composite sponges achieve a win−win situation in both efficient hemostasis and biosafety.[23,24] Moreover, graphene possesses unique a thermal conductive property.[25] Graphene aerogel is often used as an excellent substance for heat transfer or storage.[26] Therefore,

Received: March 20, 2019
Accepted: June 17, 2019

DOI: 10.1021/acsami.9b04956
ACS Appl. Mater. Interfaces XXXX, XXX, XXX−XXX

Scheme 1. Composite Strategy of the Z-CGS[a]

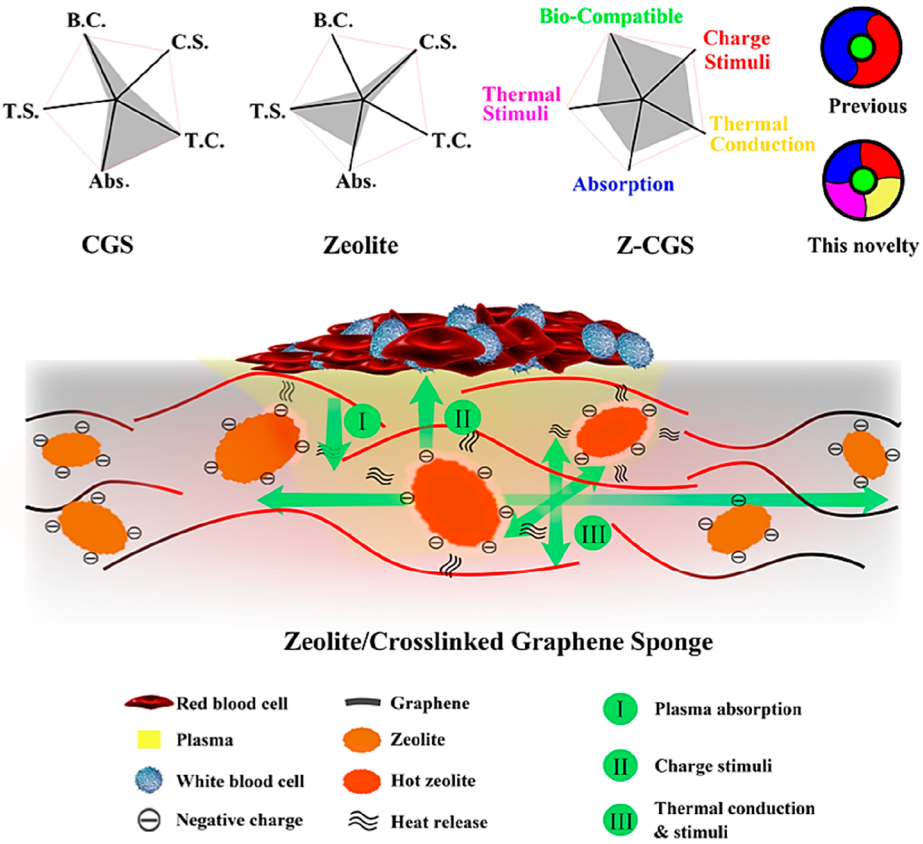

[a]The CGS possesses good biocompatibility (B.C.), fast physical absorbability (Abs.), and efficient thermal conduction (T.C.), while the zeolite possesses thermal stimulation (T.S.) and charge stimulations (C.S.). After composition, the Z-CGS inherits these properties and shows a strong comprehensive hemostatic performance. When the Z-CGS is applied to a bleeding wound, plasma is rapidly absorbed and blood cells gather on the surface of the Z-CGS. Meanwhile, the heat generated by zeolite powders is conducted to remote end by graphene sheets, and coagulation cascade is activated by the thermal and charge stimulation. Finally, via the synergistic effect of thermal stimulation, charge stimulation, and physical absorption, the Z-CGS effectively stops bleeding.

when graphene aerogel is composited with zeolite, the heat generated by zeolite can be rapidly dispersed in graphene aerogel, preventing the formation of high-temperature areas. This composite strategy suggests consideration of the wide application of zeolite in hemostasis in a new and unique way.

Here, we present a zeolite/cross-linked graphene sponge (Z-CGS) produced via one-pot hydrothermal reaction. The obtained sponge has mild exothermic process and good thermal conductivity. The thermal release of zeolite inside could be used for enhancing blood clotting, while its thermal injury is eliminated by thermal conduction of graphene (Scheme 1). On the basis of the synergistic effect of thermal, charge, and physical absorption, the Z-CGS is expected to be a multieffect trauma hemostat.

2. EXPERIMENTAL SECTION

2.1. Materials. Graphite powders (80 mesh) were purchased from Qingdao Jinrilai Co., Ltd., Shangdong, China. Sulfuric acid (H_2SO_4, 98%), sodium nitrate ($NaNO_3$, AR), potassium permanganate ($KMnO_4$, 99.9%), hydrogen peroxide (H_2O_2, 30%), and hydrochloric acid (HCl, 37%) were obtained from Sigma-Aldrich Co. The graphene oxide (GO) solution was prepared by a modified Hummers' method,[27] and the concentration of GO solution was 8 mg mL^{-1}. Zeolite was purchased from Sinopharm Chemical Reagent Co., Ltd. (Shanghai, China). Other reagents also were obtained from Sinopharm Chemical Reagent Co., Ltd., and they were used as received without any further purification.

2.2. Preparation and Characterization of the Z-CGS. Zeolite powders (200 mg) were added into 20 mL of GO solution (8 mg mL^{-1}) and sonicated for 5 min (Digital Ultrasonic Cleaner model CD 4820, 42 kHz, 160 W, Shenzhen Codyson Electrical Co., Ltd., China). After that, 0.2 mL of ethylenediamine (EDA) was added to the mixture of zeolite and GO solution. The obtained mixture needed to be sonicated for another 5 min. The obtained mixture solution was sealed in a hydrothermal synthesis reaction kettle, which was kept at 96 °C for 6 h to obtain a hydrogel. The hydrogel was frozen at −4 °C for 4 h and then moved to the inside of a freeze-dried machine for 2 days. The obtained dry hydrogel was washed in Soxhlet extractor with ethanol at 110 °C for 2 days to remove small-molecule impurities. After drying at room temperature for 24 h, 5 s puffing was applied to the composite sponge to reduce existing oxygen-containing functional groups. To obtain the final composite sponge, this sponge needed to be kept at 150 °C for 3 h. To distinguish different composite sponges prepared with 5A zeolite and ZSM-5 zeolite, we named them Z-CGS and Z-CGS_{zsm}, respectively.

Scanning electron microscopy (SEM, 7800) was employed to observe the inside structure of the Z-CGS. Energy-dispersive spectrometry (EDS, Hitachi S-4700) was used to analyze the surface element content of the Z-CGS. The liquid absorption of the Z-CGS was assessed with CGS as a control. The absorption capability was calculated according to whether the Z-CGS absorbed liquid or not. In addition, the absorption rate was scaled by recording the time that a

DOI: 10.1021/acsami.9b04956
ACS Appl. Mater. Interfaces XXXX, XXX, XXX−XXX

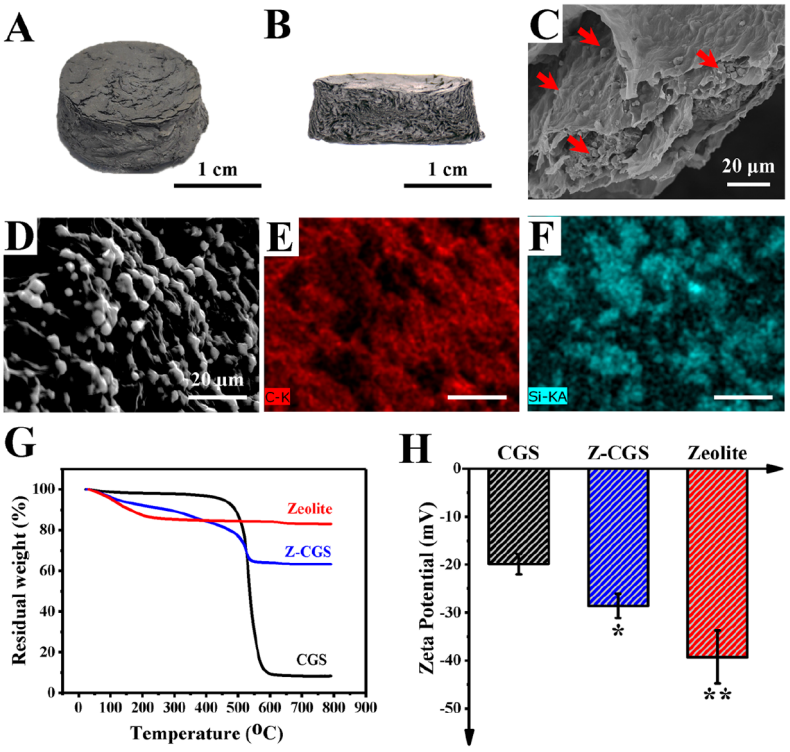

Figure 1. (A) Photograph of the Z-CGS; (B) cross section of the Z-CGS; (C) cross section SEM image of the Z-CGS. The red arrows show the anchor zeolite inside the Z-CGS. (E, F) EDS mapping of C and Al elements corresponding to (D), respectively. (G) TGA curves and (H) zeta potential of zeolite, the CGS, and the Z-CGS. Data values correspond to the mean ± SD, $n = 5$; two-way ANOVA, $*p < 0.05$, $**p < 0.01$.

liquid drop got into materials with a high-speed camera (40 ms per frame).

Fourier transform infrared (FTIR) spectra of the pure GO, the zeolite, and the Z-CGS were recorded over a wavenumber range of 4000−990 cm^{-1}. Thermogravimetric analysis (TGA, Mettler Toledo TGA/DSC1/1100SF) was used to analyze the content of zeolite powders in the Z-CGS. Zeta potential (Malvern NanoSizer ZS 2000) was employed to assess the negative potential value of the Z-CGS and the zeolite. Brunauer−Emmett−Teller (BET) surface area measurements were determined by the nitrogen gas adsorption method by using a Micromeritics ASAP 2460 2.02 analyzer at liquid nitrogen temperature. IR thermography was performed to assess the exothermic capacity of the Z-CGS with an infrared camera. The exothermic capacity of the Z-CGS was assessed with an infrared imager (FLIR E40, 64517715).

2.3. In Vitro Whole Blood Clotting Assay. The prepared samples (1 cm^2 for solid, 0.1 g for powders) were placed into glass dishes at 37 °C for 5 min. The fresh anticoagulated whole blood was obtained from SD rat; 100 μL of anticoagulated (ACD) whole blood was dropped onto each sample, followed by 10 μL of 0.2 M $CaCl_2$ solution, and then incubated at 37 °C. After 5 min, 25 mL of deionized water was dropped onto the surface without disturbing the clotted blood and incubated at 37 °C with shaking at 30 rpm for 10 min. Red blood cells without adherence on the clot were collected. The absorbance of the resultant hemoglobin solution was measured at 542 nm (Abs of samples). The ACD blood in deionized water was used as the negative reference (Abs of blank). The test was performed by employing three independent samples, and the obtained results were averaged. The blood clotting index (BCI) of the sample was calculated as follows:

$$\mathrm{BCI}\ (\%) = \frac{\mathrm{Abs}_{\mathrm{sample}}}{\mathrm{Abs}_{\mathrm{negative}}} \times 100\%$$

2.4. Hemolysis Assay In Vitro. The anticoagulated blood was obtained from SD rats. The treatment was carried out as reported to obtain the red blood cells (RBCs). To assess the hemolytic activity of materials, 0.2 mL of diluted RBCs was added into 0.8 mL of the sample suspension solutions in phosphate-buffered saline (PBS) at several concentrations (from 15.6 to 1000 μg mL^{-1}). To get the sample solutions, sample powders were added in PBS and treated with sonication for 2 h. PBS (+RBCs) and deionized water (+RBCs) were chosen as negative and positive controls. These samples were put into a rocking shaker for 3 h at 37 °C. After that, these samples were centrifuged at 10 000g for 5 min. The absorbance value of the sample solution was measured with a UV−vis spectrophotometer at 540 nm. The hemolysis rate was calculated by the following formula,

$$\text{hemolysis}\ (\%) = \frac{\mathrm{Abs}_{\mathrm{sample}} - \mathrm{Abs}_{\mathrm{negative}}}{\mathrm{Abs}_{\mathrm{positive}} - \mathrm{Abs}_{\mathrm{negative}}} \times 100\%$$

where $\mathrm{Abs}_{\mathrm{sample}}$, $\mathrm{Abs}_{\mathrm{negative}}$, and $\mathrm{Abs}_{\mathrm{positive}}$ correspond to the absorbances of the sample, negative control, and positive control, respectively.

2.5. APTT and PT Assay. The prothrombin time (PT) and activated partial thromboplastin time (APTT) were tested with MC-2000 semiautomatic coagulation analyzer (TECO, Germany). Fresh blood was collected from healthy SD rats and stored in an ACD tube with 3.8% sodium citrate. The fresh blood was centrifuged at 3000 rpm for 15 min at 4 °C, and the platelet poor plasma (PPP) was obtained by collecting the supernatant. The Z-CGS, zeolite, PPP, PT reagent, APTT reagent, and $CaCl_2$ (0.025 M) solution were incubated at 37 °C in advance. PT was performed by adding 50 μL of PPP and 100 μL of PT reagent to the sample solutions successively. To test APTT, 100 μL of PPP and 100 μL of APTT reagent were incubated at 37 °C for 5 min, and then 100 μL of $CaCl_2$ was added to each sample. Pure PPP was used as the control. All experiments were run in triplicate ($n = 3$).

2.6. Evaluation of Hemostatic Performance. The exothermic effect of materials after being applied to wound was characterized with a femoral artery model as described in reports with a slight modification. Animals were treated and cared for in accordance

DOI: 10.1021/acsami.9b04956
ACS Appl. Mater. Interfaces XXXX, XXX, XXX−XXX

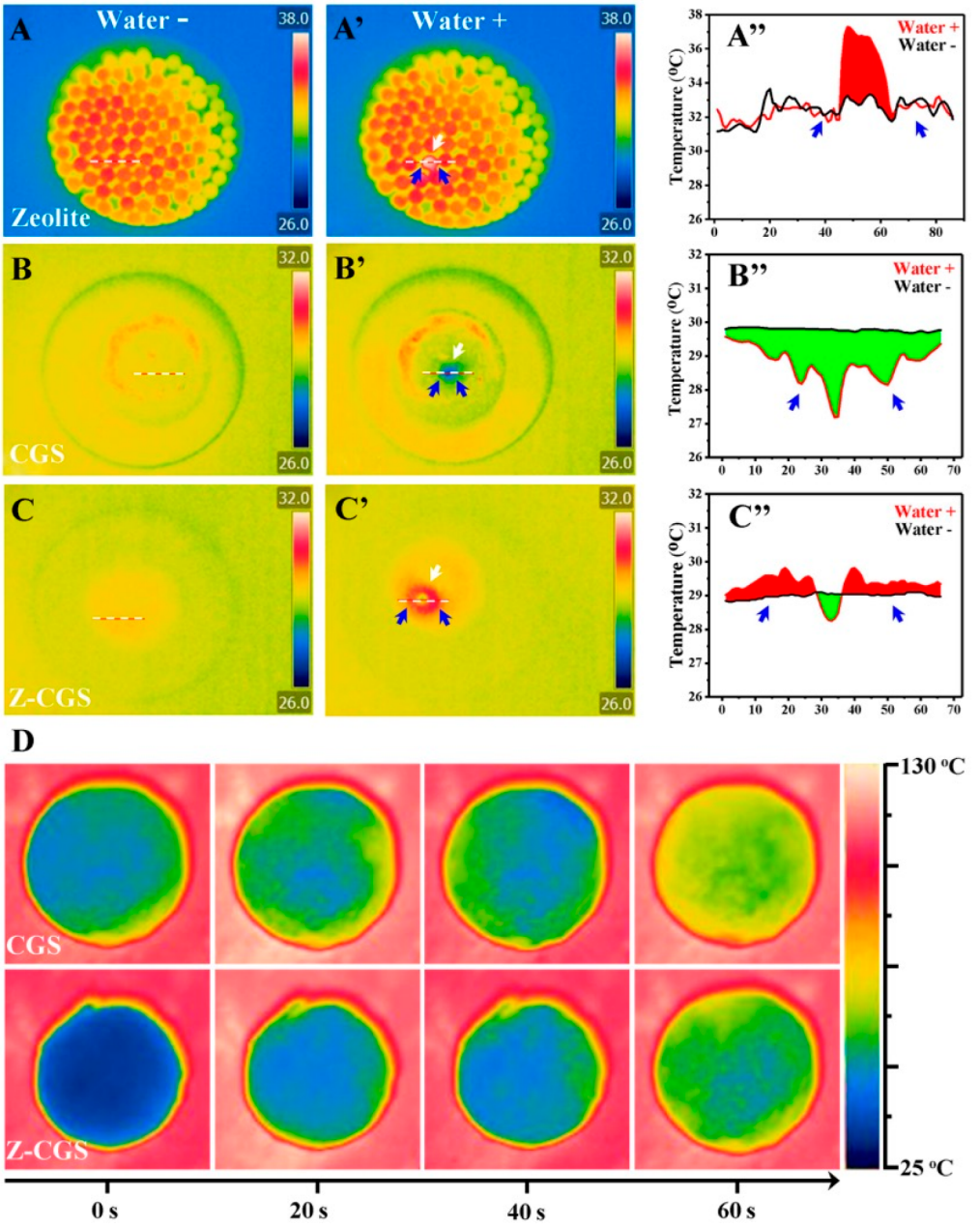

Figure 2. (A−C and A'−C') IR image and (A"−C") temperature curve before or after liquid absorption for (A) zeolite, (B) the CGS, and (C) the Z-CGS; (D) IR image of thermal conductivity for the CGS and the Z-CGS.

with the National Research Council's Guide for the care and use of laboratory animals and under the supervision and assessment by the SPF Animal Department of Clinical Institute in China−Japan Friendship Hospital (Approval no. 180202). Anesthetized SD rats were fixed on a Styrofoam tablecloth by surgical tape. One of the legs was incised, and muscle fascia was removed to expose the femoral artery. The vessel was then cut using a scalpel. After inflicting the injury, the materials were applied to the arterial wound area separately. Then, a filter paper was placed immediately below the cut to absorb the blood. The filter paper was changed every 10 s, and the wet filter paper weight was recorded to determine the total amount of bleeding and the time to cessation of bleeding. The SD rats were euthanized by cervical dislocation, and the surrounding muscle of wound was excised and fixed in 4% buffered paraformaldehyde and stained with H&E for histological analysis.

2.7. Measurement of Plasma H_2S Levels. Plasma H_2S levels at 3 h posthemostasis were measured using the fluorescent dye 7-azido-4-methylcoumarin (AzMC) as described.[28]

3. RESULTS AND DISCUSSION

3.1. Material Characterization. The composite hemostat was prepared by a facile hydrothermal reaction. The raw material is GO, which has versatile chemical reaction capability and good biocompatibility.[29−32] The obtained Z-CGS was a lightweight black sponge (Figure 1A; 2 cm diameter, 1 cm thickness) and has bubble-like layer stacking structure (Figure 1B). In the enlarged SEM image, zeolite powders were covered (the red arrows in Figure 1C) and anchored to the two-dimensional graphene sheets (Figure 1C and D) because of the rich interactions, such as hydrogen-bonding and electrostatic interactions. The size of zeolite was ∼2−4 μm. This fact was important and was the prerequisite to avoid thermal burns by preventing zeolite from contacting the wound tissue directly. Energy-dispersive spectrometry (EDS) mapping further confirmed the location of zeolite by testing the distribution

DOI: 10.1021/acsami.9b04956
ACS Appl. Mater. Interfaces XXXX, XXX, XXX−XXX

of Si elements (Figure 1D and E). In Figure S1, the Fourier transform infrared (FTIR) spectra presented the changes in functional groups during material preparation. These changes of absorption peaks in 3417, 1743, and 1585 cm^{-1} verified the assembly of graphene sheets,[33,34] and the strong absorption at 1014 cm^{-1} confirmed the existence of zeolite. All these results demonstrated that the ideal composite sponge was prepared successfully.

The composition of the Z-CGS was assessed by TGA test (Figure 1G). According to the TGA curves, the Z-CGS contained 63.26% indecomposable and 36.74% decomposable ingredients after 800 °C calcination. The decomposable ingredients may be the organic part of the Z-CGS, while the indecomposable ingredients were attributed to the indecomposable parts of the CGS and zeolite. The indecomposable parts of CGS and zeolite were tested to be 82.92% and 8.36%, respectively. Therefore, according to the percentage of the decomposable parts and the indecomposable parts, it could be calculated that the Z-CGS contained about 73.63% w/w (14.81%, v/v) zeolite powders. These results are consistent with their potential changes (Figure 1H). The Malvern Nanosizer zs 2000 was employed to detect the zeta potential of zeolite, Z-CGS, and CGS.[35−37] Zeolite has a negative surface charge, and its zeta potential is −39.28 ± 2.10 mV. The addition of zeolite decreased the zeta potential of the Z-CGS, which decreased to −28.58 ± 2.54 mV from −19.9 ± 2.1 mV of the original CGS. Previous studies confirmed that potential is one of the important hemostatic stimulations.[22−24] The decrease of negative charge will afford stronger stimulation for hemostatic factors and blood cells. As a result, the activated factors and blood cells trigger the coagulation cascade and achieve hemostasis. Therefore, we deduced that this composite sponge, to a large extent, would accelerate blood coagulation. On the basis of the data of the N_2 adsorption−desorption isotherm of Z-CGS, the calculated BET surface area of Z-CGS was 39.8 m^2 g^{-1}, and its pore size distribution mainly concentrated at 3.63 nm. Zeolite was a micromesopured structure with a pore size distribution between 0.5−4 nm (average pore diameter was 0.75 nm, Figure S2). A previous study reported that the pore distribution of CGS was relatively wide, ranging from 0 to 100 nm (average pore diameter was 5.7 nm).[21] When zeolite was composited to the CGS, the pore size distribution of the obtained Z-CGS mainly concentrated at 3.63 nm. The response value (dV) was strong, which was similar to that of zeolite. The results indicated that the average pore diameter of Z-CGS was mainly provided by the zeolite. At the same time, the smaller pore signal of zeolite in the Z-CGS was relatively weakened. This meant that, during the hydrothermal reaction, the residual cross-linker (EDA) and water would occupy the inner space of the zeolite.

Zeolite Linde type 5A is a high surface area crystalline molecular sieve that releases heat upon water absorption.[11,15] After the hydrothermal reaction, the zeolite powders inside the Z-CGS fully hydrated and lost the exothermic capacity. Thermal dehydration is a common method to restore the heat release capacity of zeolite. As Figure S3 presents, ∼65% (w/w) of water inside the fully hydrated zeolite was removed after 100 °C high-temperature treatment for 1 h. Prolonging the time did not help with dehydration; with increased heating temperature, the water content of the Z-CGS decreased sharply. After 150 °C treatment for 3 h, 95% (w/w) of water could be removed. The obtained zeolite restored 50% thermal release capacity. Although higher treatment temperature could remove water thoroughly, the exothermal capacity of the obtained zeolite was slightly improved. Additionally, the processed temperature exceeding 200 °C could destroy the Z-CGS structure and weaken its liquid absorbability, which was not conducive to hemostasis. Therefore, the final sponge was obtained by 150 °C treatment for 3 h.

3.2. Thermal Capacity Assessments of Z-CGS. The exothermic capacity of different materials was recorded by an infrared imager (IR) (Figure 2A−C). When zeolite particles were exposed to the environment, they could release heat as absorbing water vapor. Thus, we could see that the temperature of zeolite particles was higher than the environment temperature (Figure 2A). When 1 μL of water was injected on the surface of a zeolite particle, it quickly absorbed water and rapidly released heat (marked with white arrows in Figure 2A'). The released amount was related to the absorbed water content. Through just adding 1 μL of water, the local temperature of the zeolite particle could rise by 4 °C (red area in Figure 2A"), suggesting stronger exothermal capacity of zeolite. In contrary, the CGS is not exothermic. When the CGS absorbed water, the overall temperature of the surrounding region got down to ∼0.5 °C because of the evaporation of water (Figure 2B−B"). For the Z-CGS, it exhibited obviously exothermal reaction upon water absorption. As shown in Figure 2C−C', a distinct heat ring formed around the water droplet. The heat was transferred from the center to the periphery. The temperature change before and after water absorption was up to 1 °C (Figure 2C"), indicating that the Z-CGS successfully inherited the exothermal capacity. For quantitative analysis of the exothermal capacity, the Z-CGS was immersed in water, and its thermal release was monitored. The exothermic capability of the Z-CGS was tested to be 10.199 ± 0.138 °C g^{-1} mL^{-1}, which was slightly lower than that of the naked zeolite (39.674 ± 2.107 °C g^{-1} mL^{-1}, Figure S4). The decreased heat-release capacity of the Z-CGS could be attributed to two factors: (1) the residual EDA and moisture and (2) the coverage of zeolite by graphene-based nanosheets. These factors may affect the hydration capacity of the Z-CGS that further decreased its heat-release capacity. Additionally, zeolite content in the Z-CGS was ∼73.63%, and the other component of the Z-CGS did not have the ability to release heat. As a result, the exothermic capability of the Z-CGS was slightly weakened. Regardless, the exothermic capability of the Z-CGS was enough for providing heat stimulation of hemostasis. It should be considered that the exothermic process of the Z-CGS would give rise to local high temperature, which may cause thermal injury. Therefore, good heat transfer of the Z-CGS is important to prevent the formation of local high temperature.

Figure 2D presents the thermal conductivity test of the CGS and the Z-CGS (5 mm thickness). Both the CGS and the Z-CGS were placed on a hot plate with 130 °C high temperature. With prolonged heating time, thermal was transferred from the plate to the materials. Their heat transfer rapidly reached equilibrium within 60 s (Figure 2D), suggesting excellent heat-transfer ability of the Z-CGS and the CGS.[25,38,39] Compared with the CGS, the Z-CGS exhibited a slight hysteresis effect in heat transfer and a lower temperature on the surface. This phenomenon was in accord with the actual situation that zeolite powders are not heat-transfer materials, and their addition would attenuate transfer ability of the Z-CGS. Overall, all these results demonstrated that the composite strategy of the Z-CGS was successful. The zeolite inside the Z-CGS

DOI: 10.1021/acsami.9b04956
ACS Appl. Mater. Interfaces XXXX, XXX, XXX−XXX

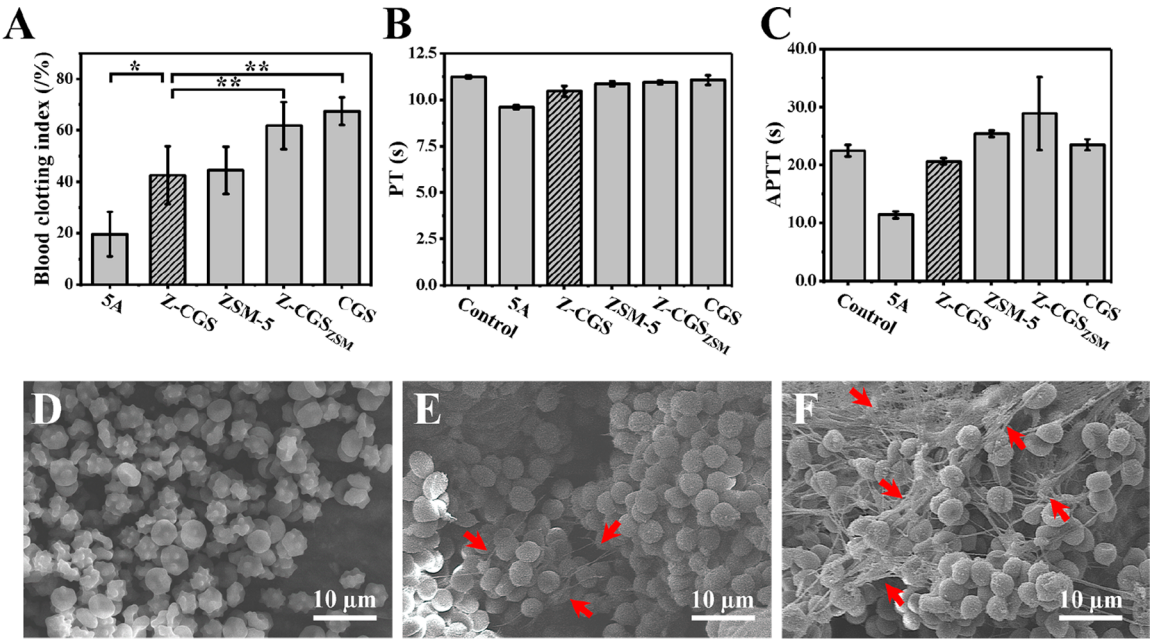

Figure 3. (A) BCI test, (B) PT, and (C) APTT of 5A zeolite, ZSM-5 zeolite, the Z-CGS, the Z-CGS$_{zsm}$, and the CGS (data values correspond to the mean ± SD, $n = 6$; two-way ANOVA, *$p < 0.05$, **$p < 0.01$). SEM images of interfacial interaction between blood cells and hemostat: (D) the CGS, (E) the Z-CGS$_{zsm}$, and (F) the Z-CGS.

exerted exothermal capacity, while the CGS played pivotal roles in heat transfer, preventing the formation of local high-temperature area.

Aside from thermal stimulation, the liquid absorbability of the Z-CGS was also investigated. It is another key factor for hemostatic performance. Earlier studies revealed that reducing thermal injury by hydration would attenuate the hemostatic performance of zeolite because of the accompanied weaken absorbability.[40,41] However, for the Z-CGS composite, this limitation could be removed. Graphene-based sponge has remarkable liquid absorption; the Z-CGS could be considered as an infinite space compared with the limited tank of the zeolite powder. Figure S5 presented the liquid absorption data of Z-CGS and CGS. The liquid absorption amounts of the Z-CGS were 830.3 ± 8.8 mg cm^{-3} (water) and 771.9 ± 25.1 mg cm^{-3} (blood), which were similar to those of the CGS (955.4 ± 59 mg cm^{-3} for water and 1226.7 ± 35.4 mg cm^{-3} for blood). The Z-CGS absorbed a liquid droplet within 120 ms (water) and 360 ms (blood), which was a little slower than the CGS (40 ms for water or blood).[21] This fact was mainly due to zeolite particles occupying the interior space, which weakened the liquid absorption ability of the Z-CGS. As shown in Figure S6, while increasing the dose of zeolite, the absorption capacity of the composite sponge further decreased, which was not conducive to the hemostatic performance. In contrast, when the dose of zeolite decreased, the thermal capacity of the Z-CGS decreased sharply (Figure S7). Thus, the target composite sponge was prepared with zeolite powders and GO in the ratio of 10/1 (w/v).

3.3. Hemostatic Performance In Vitro. Up to now, the debates about the role of heat in hemostasis still exist.[16−20] To clarify the effect of the thermal stimulation on the hemostatic performance of the Z-CGS, the blood clotting index (BCI) test was conducted. ZSM-5 was used as a control for 5A (named zeolite in the manuscript) because both of them have the same MFI framework and similar element composition. The main difference is that 5A zeolite has the exothermal capability, while ZSM-5 zeolite does not. As shown in Figure 3A, the BCI of 5A zeolite was significantly lower than that of ZSM-5 zeolite, which confirmed that proper exothermic reaction accelerated blood clotting. When ZSM-5 was embedded into the CGS, the obtained Z-CGS$_{zsm}$ showed better blood-coagulation performance than the CGS. This result was mainly due to the synthetic effect of charge stimulation of ZSM-5 and physical absorption of the CGS, which was also consistent with our previous studies.[23] Compared with the Z-CGS$_{zsm}$, the Z-CGS possessed not only the properties of charge stimulation and physical absorption but also exothermic stimulation. Therefore, under the ternary synergy effect, the Z-CGS significantly reduced the BCI value to 40% and exhibited the best blood clotting performance. These results demonstrated that exothermic stimulation was in favor of promoting hemostasis. To find out how the exothermic stimulation improves hemostasis, the blood-coagulation cascade of the Z-CGS was investigated. The blood-coagulation cascade contains intrinsic pathway and extrinsic pathway. The prothrombin time (PT) is the time required for a fibrin clot to form after adding tissue thromboplastin, showing the performance of the extrinsic coagulation pathway. Activated partial thromboplastin time (APTT) is the time required for a fibrin clot to form after the clotting process is initiated by adding a partial thromboplastin reagent and $CaCl_2$ solution, exhibiting the performance of the intrinsic coagulation pathway.[42,43] The PT and APTT of zeolite dropped to 9.60 and 11.40 s from 11.23 and 22.47 s, respectively, when taking pure PPP as control, while ZSM-5 just slightly reduced the PT time. When clay was embedded to graphene sheets, the PT and APTT of the Z-CGS were reduced to 10.47 and 20.63 s, respectively. These results further verified that the Z-CGS accelerated blood coagulation by the activation of the extrinsic pathway of the coagulation cascade.

Additionally, either in extrinsic or intrinsic coagulation pathway, thrombin would be activated and trigger the formation of fibrin at the downstream.[44] Therefore, to

DOI: 10.1021/acsami.9b04956
ACS Appl. Mater. Interfaces XXXX, XXX, XXX−XXX

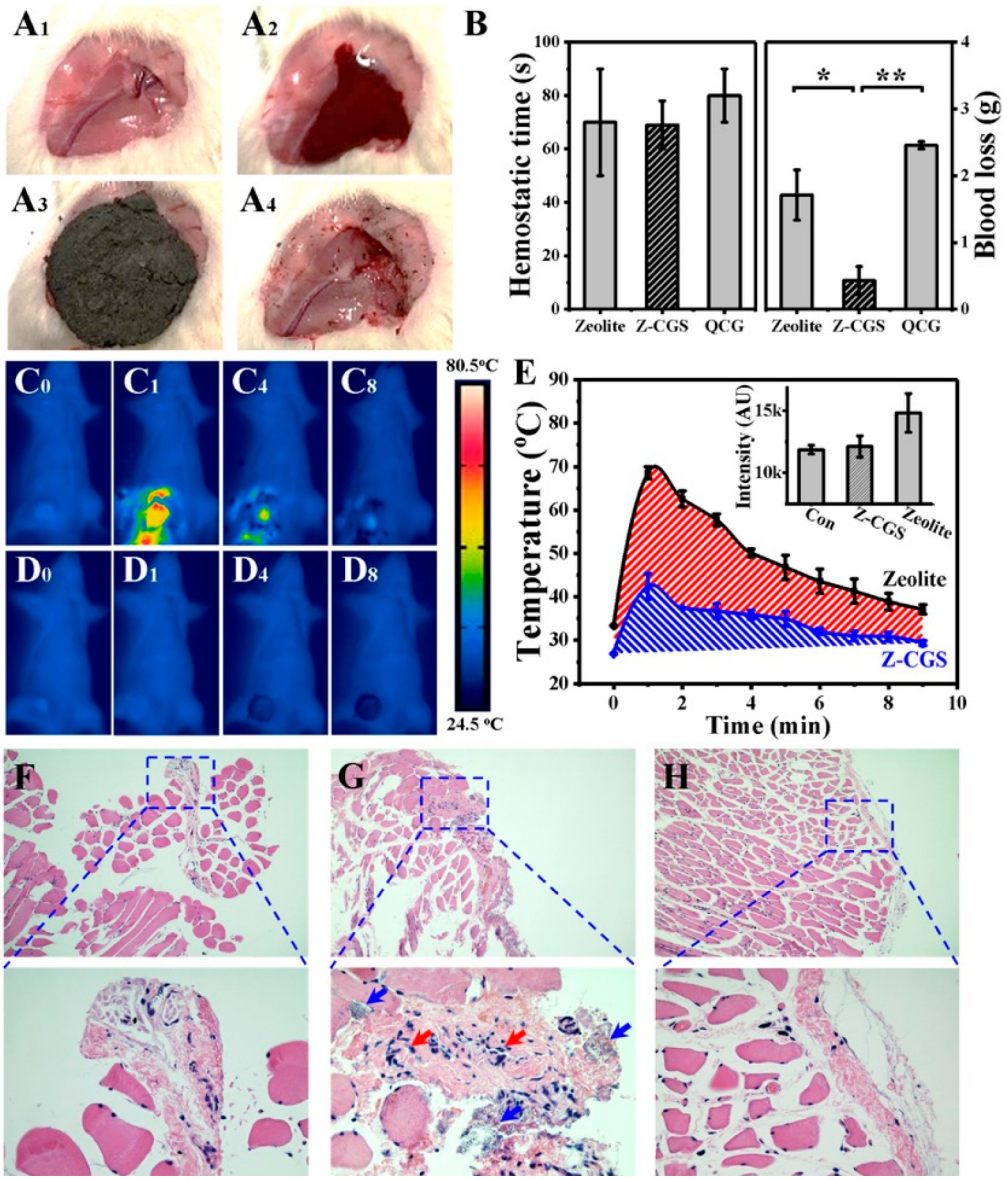

Figure 4. (A) Hemostatic experiment in SD rat artery injury model. (B) Hemostatic time of the Z-CGS and the zeolite in the SD rat artery injury model (data values correspond to the mean ± SD, $n > 3$; two-way ANOVA, $^{*}P < 0.05$, $^{**}p < 0.01$). IR images of hemostatic process in the SD rat artery injury model: (C) the zeolite and (D) the Z-CGS. The subscripts show the time since the hemostat was applied to the wound. (E) Temperature curve of wound tissue after application of different hemostats. The inset shows the H_2S expression levels in different groups by testing fluorescence intensity. Histological analysis of healed wounds: (F) control, (G) the zeolite, and (H) the Z-CGS.

intuitively verify the coagulated stimulation of the Z-CGS, the interfacial interaction between blood cells and different materials was observed with SEM (Figure 3D and E). The Z-CGS rapidly absorbed plasma, leaving blood cells and platelets gathered on the surface (Figure 3F). With the thermal stimulation and charge stimulation, platelets were activated and triggered the formation of fibrin. As such, a larger amount of insoluble fibrin was found on the surface of the Z-CGS, and the fibrin built up a firm network with blood cells together (red arrows in Figure 3F). Interestingly, although the Z-CGS$_{zsm}$ could also trigger the formation of fibrin via charge stimulation (Figure 3E), the fibrin amount of the Z-CGS$_{zsm}$ was significantly lower than that of the Z-CGS. As a control group, the CGS only possessed physical absorbability that enriched blood cells and platelets on its surface, but it could not induce fibrin formation (Figure 3D).[44] These results were consistent with BCI data that heat release played a positive role in hemostasis. The Z-CGS displayed thermal stimulation, charge stimulation, and physical absorbability during the hemostatic process. In the synergy of these triple effects, the Z-CGS showed better hemostatic capacity than the Z-CGS$_{zsm}$ and the CGS. It was also the first time to integrate three coagulated stimulations into graphene-based hemostat.

3.4. Hemostatic Performance In Vivo and Cytotoxicity Evaluation. The in vivo hemostatic performance of the Z-CGS was evaluated using an SD rat artery injury model. The commercial QuikClot Combat Gauze (QCG), which is the standard hemostatic agent in the U.S. military recommended by the *Committee on Tactical Combat Casualty Care*,[12] was used as the control. Figure 4A presents the process of hemostasis. SD rats (weight 250 ± 20 g) were used as the experimental animals ($n > 3$). First, the skin and fascia were excised to

DOI: 10.1021/acsami.9b04956
ACS Appl. Mater. Interfaces XXXX, XXX, XXX−XXX

expose the artery (Figure 4A$_1$); the damage was created at the artery (Figure 4A$_2$); different hemostats were applied to wound (Figure 4A$_3$); as hemostasis completed, the wound was cleared with saline (Figure 4A$_4$). As a standard hemostat, the QCG achieved hemostasis in 80 ± 10 s. Compared to the QCG, the Z-CGS had a short hemostatic time of 69 ± 9 s, which showed no difference with the naked zeolite powders (70 ± 20 s, Figure 4B). These results demonstrated that the Z-CGS has a more powerful hemostatic capacity than the QCG. Additionally, the blood loss of the Z-CGS was 0.43 ± 0.21 g, which was significantly lower than those of zeolite powders (1.71 ± 0.38 g, $P < 0.05$) and the QCG (2.46 ± 0.06 g, $p < 0.01$). As reported, the blood volume of an adult SD rat is ~6.4 mL/100 g.[45] A 250 g healthy SD rat contains 16 g of blood in its body. When a healthy SD rat loses 2.5 g (15.6%) of blood, its heart and respiratory rates would increase and the blood pressure would decrease.[46] When humans lose 15.6% of their blood, this amount of loss increases the heart and respiratory rates and decreases the urine output and blood pressure. Besides, the skin may become cooler and pale. This fact was essential for saving lives by preventing significant blood loss, which could cause serious complications. During the hemostatic process, we found that the wound would rebleed when zeolite powders or the QCG was removed. Conversely, the use of the Z-CGS avoided the occurrence of rebleeding during debridement. As reported, people feel uncomfortable when seeing red blood, and 3%−4% of people even suffer from blood phobia.[47] For traditional hemostats, the hemostat is red after hemostasis. This may cause psychological stress or even sickness to the patient. In contrast, the obtained Z-CGS was a lightweight black sponge. The black appearance of Z-CGS masks the red color of the blood after hemostasis, and this will make patients feel better (Figure 4A$_3$).

Importantly, the use of zeolite powders caused serious burns when they were applied to a bleeding wound.[48] The IR record showed that the surrounding tissue was heated to a high temperature of 70 °C in the first minute (Figure 4C and D; the whole process is provided in Figure S8). The temperature dropped slowly, and the high temperature lasted for 9 min. Previous studies revealed that an adult human perceives pain when the skin temperature is >43 °C. When the basal layer of the epidermis reaches 44 °C, burn injury occurs. Once beyond 70 °C, the rate of damage is rapid and thermal injury is serious.[49] It could be seen that the direct use of zeolite has a serious side effect. That was also the reason why zeolite was replaced in the hemostatic application. Conversely, the use of the Z-CGS did not give rise to obvious local high temperature. During the whole hemostatic process, the Z-CGS presented a milder exothermic reaction, and wound tissue temperature was kept at 42 °C for 1 min (Figure 4D and E). It was more conducive to activate factors to accelerate blood clotting instead of burning wound tissue. The heat released by the Z-CGS kept wound tissue warm for 4 min, which was beneficial for wound healing.[50] In burn models, the increase of H_2S level is the signal of tissue injury and inflammatory response.[51−53] The application of zeolite led an increase in plasma H_2S levels (fluorescence intensity was 14 844.33 ± 1 564.62; the inset in Figure 4E), which was assessed by the fluorescent dye 7-azido-4-methylcoumarin (AzMC). Differently, no fluorescent intensity increased in the Z-CGS group (12 135.33 ± 859.41) compared with the normal plasma as control (11 882.00 ± 355.52). Therefore, these results demonstrated that the Z-CGS could effectively manage the exothermic reaction of zeolite and make it useful in hemostasis.

The biocompatibility of the Z-CGS was investigated by histological analysis (H&E), hemolysis evaluation, and cytocompatibility assessment. The thorough removal of the granular hemostatic agent was difficult.[11] As shown in Figure 4G, residual zeolite (marked with blue arrows) was observed in the image of H&E staining. Meanwhile, the aggregation of inflammatory cells in connective tissue (marked with red arrows) suggested the thermal damage of wound. Compared with the naked zeolite, the Z-CGS had little materials residue. No aggregation of inflammatory cells was found, and wound tissue kept a normal form, the same as the control group (Figure 4F and H). Hemolysis test was carried out to access the hemocompatibility of materials, and the results are presented in Figure S9. The naked zeolite could result in dose-dependent development of hemoglobin. About 1000 μg mL^{-1} dose of zeolite caused 5.7 ± 0.4% hemolysis. Zeolite embedded into graphene sheets led to better blood compatibility. Only 2.6 ± 0.4% hemolysis happened when the dose of zeolite was up to 1000 μg mL^{-1}. This result further confirmed that graphene-based sponge was a novel platform to eliminate side effects. The impact of thermal stimulation on cell compatibility was investigated by cell coculture in vitro. L929 cells were chosen to assess the cells compatibility of the Z-CGS.[54,55] As Figure S10 shows, no visible differences were observed in different groups. By increasing the addition dose of each group, cells still maintained a regular form and kept normal growth. These evaluations indicated that the Z-CGS had a good biocompatibility.

4. CONCLUSION

In summary, we developed a new hemostatic sponge (Z-CGS) by a facile composite strategy. The graphene sheets constituted the porous framework of the Z-CGS and wrapped zeolite powders tightly by their two-dimensional structure. Good thermal conduction of graphene effectively prevented thermal injury caused by zeolite (<42 °C) and applied thermal stimulation to trigger blood coagulation. On the synergy effects of thermal stimulation, charge stimulation, and physical adsorption, the Z-CGS achieved outstanding hemostatic performance. Bleeding was stopped within 69 s in rat artery injury model, which was 11 s faster than that of the commercial QCG. Blood loss of the Z-CGS was 0.43 g, which was significantly lower than those of zeolite powders (1.71 g) and the QCG (2.46 g). Additionally, cytotoxicity assay and pathological analysis further confirmed the good biocompatibility of the Z-CGS. Therefore, Z-CGS is an outstanding hemostat. It combines the advantages of zeolite and graphene while getting rid of the shortcomings of the basic unit, achieving a win−win situation in both efficiency hemostasis and biosafety. Compared to traditional hemostats, the Z-CGS has many advantages, such as facile preparation, low cost, portability, long shelf life, outstanding absorbability, good biocompatibility, being antimicrobial, and comfortable usage owing to the black color.[56,57] Therefore, we anticipate that this work could not only provide a unique method for safe and highly efficient use of zeolite in hemostasis but also provide a new perspective to develop a novel hemostat used for trauma therapy.

DOI: 10.1021/acsami.9b04956
ACS Appl. Mater. Interfaces XXXX, XXX, XXX−XXX

■ ASSOCIATED CONTENT

Supporting Information

The Supporting Information is available free of charge on the ACS Publications website at DOI: 10.1021/acsami.9b04956.

Material characterization including FTIR, N_2 adsorption−desorption isotherm, BJH pore size distribution, thermal dehydration, heat-release capacity, exothermic capacity, liquid absorbability, IR images, hemolysis rate, and cytocompatibility (PDF)

■ AUTHOR INFORMATION

Corresponding Authors

*E-mail: chase.lg@163.com.

*E-mail: wangxing@mail.buct.edu.cn.

ORCID

Xing Wang: 0000-0002-9990-1479

Notes

The authors declare no competing financial interest.

■ ACKNOWLEDGMENTS

The authors thank the National Natural Science Foundation of China (21574008), China Postdoctoral Science Foundation Funded Project (2018M641162), and the Fundamental Research Funds for the Central Universities (BHYC1705B and PYBZ1806) for their financial support.

■ REFERENCES

(1) Zhao, X.; Guo, B.; Wu, H.; Liang, Y.; Ma, P. X. Injectable Antibacterial Conductive Nanocomposite Cryogels with Rapid Shape Recovery for Noncompressible Hemorrhage and Wound Healing. *Nat. Commun.* **2018**, *9*, 2784−2800.

(2) Wen, J.; Weinhart, M.; Lai, B.; Kizhakkedathu, J.; Brooks, D. Reversible Hemostatic Properties of Sulfabetaine/Quaternary Ammonium Modified Hyperbranched Polyglycerol. *Biomaterials* **2016**, *86*, 42−55.

(3) Long, M.; Zhang, Y.; Huang, P.; Chang, S.; Hu, Y.; Yang, Q.; Mao, L.; Yang, H. Emerging Nanoclay Composite for Effective Hemostasis. *Adv. Funct. Mater.* **2018**, *28*, 1704452−1704460.

(4) Saporito, F.; Sandri, G.; Rossi, S.; Bonferoni, M. C.; Riva, F.; Malavasi, L.; Caramella, C.; Ferrari, F. Freeze Dried Chitosan Acetate Dressings with Glycosaminoglycans and Traxenamic Acid. *Carbohydr. Polym.* **2018**, *184*, 408−417.

(5) Cheng, F.; Liu, C.; Wei, X.; Yan, T.; Li, H.; He, J.; Huang, Y. Preparation and Characterization of 2,2,6,6-Tetramethylpiperidine-1-oxyl (TEMPO)-Oxidized Cellulose Nanocrystal/Alginate Biodegradable Composite Dressing for Hemostasis Applications. *ACS Sustainable Chem. Eng.* **2017**, *5*, 3819−3828.

(6) Shander, A.; Kaplan, L. J.; Harris, M. T.; Gross, I.; Nagarsheth, N. P.; Nemeth, J.; Ozawa, S.; Riley, J. B.; Ashton, M.; Ferraris, V. A. Topical Hemostatic Therapy in Surgery: Bridging the Knowledge and Practice Gap. *J. Am. Coll. Surgeons* **2014**, *219*, 570−579.

(7) Alam, H. B.; Chen, Z.; Jaskille, A.; Querol, R. I. L. C.; Koustova, E.; Inocencio, R.; Conran, R.; Seufert, A.; Ariaban, N.; Toruno, K.; Rhee, P. Application of A Zeolite Hemostatic Agent Achieves 100% Survival in A Lethal Model of Complex Groin Injury in Swine. *J. Trauma* **2004**, *56*, 974−983.

(8) Kozen, B. G.; Kircher, S. J.; Henao, J.; Godinez, F. S.; Johnson, A. S. An Alternative Hemostatic Dressing: Comparison of CELOX, HemCon, and QuikClot. *Acad. Emerg. Med.* **2008**, *15*, 74−81.

(9) Rhee, P.; Brown, C.; Martin, M.; Salim, A.; Plurad, D.; Green, D.; Chambers, L.; Demetriades, D.; Velmahos, G.; Alam, H. QuikClot Use In Trauma for Hemorrhage Control: Case Series of 103 Documented Uses. *J. Trauma* **2008**, *64*, 1093−1099.

(10) Li, J.; Cao, W.; Lv, X.; Jiang, L.; Li, Y.; Li, W.; Chen, S.; Li, X. Zeolite-based Hemostat QuikClot Releases Calcium into Blood and Promotes Blood Coagulation in Vitro. *Acta Pharmacol. Sin.* **2013**, *34*, 367−372.

(11) Ahuja, N.; Ostomel, T. A.; Rhee, P.; Stucky, G. D.; Conran, R.; Chen, Z.; Al-Mubarak, G. A.; Velmahos, G.; Demoya, M.; Alam, H. B. Testing of Modified Zeolite Hemostatic Dressings in A Large Animal Model of Lethal Groin Injury. *J. Trauma* **2006**, *61*, 1312−1320.

(12) Gegel, B. T.; Austin, P. N.; Johnson, A. D. An Evidence-Based Review of the Use of A Combat Gauze (QuikClot) for Hemorrhage Control. *AANA J.* **2013**, *81*, 453−458.

(13) Carraway, J. W.; Kent, D.; Young, K.; Cole, A.; Friedman, R.; Ward, K. R. Comparison of A New Mineral Based Hemostatic Agent To A Commercially Available Granular Zeolite Agent for Hemostasis in A Swine Model of Lethal Extremity Arterial Hemorrhage. *Resuscitation* **2008**, *78*, 230−235.

(14) Kontori, E.; Perraki, T.; Tsivilis, S.; Kakali, G. Zeolite Blended Cements: Evaluation of Their Hydration Rate By Means of Thermal Analysis. *J. Therm. Anal. Calorim.* **2009**, *96*, 993−998.

(15) Devlin, J. J.; Kircher, S.; Kozen, B. G.; Littlejohn, L. F.; Johnson, A. S. Comparison of ChitoFlex®, CELOX, and QuikClot® in Control of Hemorrhage. *J. Emerg. Med.* **2011**, *41*, 237−245.

(16) Smith, A. H.; Laird, C.; Porter, K.; Bloch, M. Haemostatic Dressings in Prehospital Care. *Emerg. Med. J.* **2013**, *30*, 784−789.

(17) While, J. G. Effects of Heat on Platelet Structure and Function. *Blood* **1968**, *32*, 324−335.

(18) Gader, A. M. A.; Al-Mashhadani, S. A.; Al-Harthy, S. S. Direct Activation of Platelets by Heat Is the Possible Trigger of the Coagulopathy of Heat Stroke. *Br. J. Haematol.* **1990**, *74*, 86−92.

(19) Keatinge, W. R.; Coleshaw, S. R. K.; Easton, J. C.; Cotter, F.; Mattock, M. B.; Chelliah, R. Increased Platelet and Red Cell Counts, Blood Viscosity, and Plasma Cholesterol Levels During Heat Stress, and Mortality From Coronary and Cerebral Thrombosis. *Am. J. Med.* **1986**, *81*, 795−800.

(20) Kupchak, B. R.; Kazman, J. B.; Vingren, J. L.; Levitt, D. E.; Lee, E. C.; Williamson, K. H.; Armstrong, L. E.; Deuster, P. A. Blood Hemostatic Changes During an Ultraendurance Road Cycling Event in A Hot Environment. *Wild. Environ. Med.* **2017**, *28*, 197−206.

(21) Quan, K.; Li, G.; Luan, D.; Yuan, Q.; Tao, L.; Wang, X. Black Hemostatic Sponge Based on Facile Prepared Cross-Linked Graphene. *Colloids Surf., B* **2015**, *132*, 27−33.

(22) Quan, K.; Li, G.; Tao, L.; Xie, Q.; Yuan, Q.; Wang, X. Diaminopropionic Acid Reinforced Graphene Sponge and Its Use for Hemostasis. *ACS Appl. Mater. Interfaces* **2016**, *8*, 7666−7673.

(23) Li, G.; Quan, K.; Liang, Y.; Li, T.; Yuan, Q.; Tao, L.; Xie, Q.; Wang, X. Graphene-Montmorillonite Composite Sponge for Safe and Effective Hemostasis. *ACS Appl. Mater. Interfaces* **2016**, *8*, 35071−35080.

(24) Liang, Y.; Xu, C.; Li, G.; Liu, T.; Liang, J. F.; Wang, X. Graphene-Kaolin Composite Sponge for Rapid and Riskless Hemostasis. *Colloids Surf., B* **2018**, *169*, 168−175.

(25) Zhang, Q.; Hao, M.; Xu, X.; Xiong, G.; Li, H.; Fisher, T. S. Flyweight 3D Graphene Scaffolds with Microinterface Barrier-Derived Tunable Thermal Insulation and Flame Retardancy. *ACS Appl. Mater. Interfaces* **2017**, *9*, 14232−14241.

(26) Yan, Z.; Yao, W.; Hu, L.; Liu, D.; Wang, C.; Lee, C. Progress in the Preparation and Application of Three-dimensional Graphene-based Porous Nanocomposites. *Nanoscale* **2015**, *7*, 5563−5577.

(27) Hummers, W. S.; Offeman, R. E. Preparation of Graphitic Oxide. *J. Am. Chem. Soc.* **1958**, *80*, 1339−1339.

(28) Brunyanszki, A.; Erdelyi, K.; Szczesny, B.; Olah, G.; Salomao, R.; Herndon, D. N.; Szabo, C. Upregulation and Mitochondrial Sequestration of Hemoglobin Occur in Circulating Leukocytes during Critical Illness, Conferring a Cytoprotective Phenotype. *Mol. Med.* **2015**, *21*, 666−675.

(29) Zhang, X.; Wang, K.; Liu, M.; Zhang, X.; Tao, L.; Chen, Y.; Wei, Y. Polymeric AIE-based Nanoprobes for Biomedical Applications: Recent Advances and Perspectives. *Nanoscale* **2015**, *7*, 11486−11508.

(30) Zhang, X.; Hu, W.; Li, J.; Tao, L.; Wei, Y. A Comparative Study of Cellular Uptake and Cytotoxicity of Multi-walled Carbon

DOI: 10.1021/acsami.9b04956
ACS Appl. Mater. Interfaces XXXX, XXX, XXX−XXX

Nanotubes, Graphene Oxide, and Nanodiamond. *Toxicology Research* **2012**, *1* (1), 62−68.
(31) Zhang, X.; Yin, J.; Peng, C.; Hu, W.; Zhu, Z.; Li, W.; Fan, C.; Huang, Q. Distribution and Biocompatibility Studies of Graphene Oxide in Mice after Intravenous Administration. *Carbon* **2011**, *49* (3), 986−995.
(32) Zhang, X.; Wang, S.; Xu, L.; Feng, L.; Ji, Y.; Tao, L.; Li, S.; Wei, Y. Biocompatible Polydopamine Fluorescent Organic Nanoparticles: Facile Preparation and Cell Imaging. *Nanoscale* **2012**, *4* (18), 5581−5584.
(33) Kim, N. H.; Kuila, T.; Lee, J. H. Simultaneous Reduction, Functionalization and Stitching of Graphene Oxide with Ethylenediamine for Composites Application. *J. Mater. Chem. A* **2013**, *1*, 1349−1358.
(34) Zhang, X.; Hu, W.; Li, J.; Tao, L.; Wei, Y. A Comparative Study of Cellular Uptake and Cytotoxicity of Multi-walled Carbon Nanotubes, Graphene Oxide, and Nanodiamond. *Toxicol. Res.* **2012**, *1*, 62−68.
(35) Baker, S. E.; Sawvel, A. M.; Zheng, N.; Stucky, G. D. Controlling Bioprocesses with Inorganic Surfaces: Layered Clay Hemostatic Agents. *Chem. Mater.* **2007**, *19* (18), 4390−4392.
(36) Vogel, R.; Pal, A.; Jambhrunkar, S.; Patel, P.; Thakur, S.; Reátegui, E.; Parekh, H.; Saá, P.; Stassinopoulos, A.; Broom, M. High-resolution Single Particle Zeta Potential Characterisation of Biological Nanoparticles Using Tunable Resistive Pulse Sensing. *Sci. rep.* **2017**, *7*, 17479.
(37) Lee, H.-K.; Lee, H.-Y.; Jeon, J.-M. Codeposition of Micro-and Nano-sized SiC Particles in the Nickel Matrix Composite Coatings Bbtained by Electroplating. *Surf. Coat. Technol.* **2007**, *201*, 4711−4717.
(38) Zhang, Q.; Zhang, B.; Yu, Y.; Zhao, K.; He, P.; Huang, B. Fluoroalkyl-silane-modified 3D Graphene Foam with Improved Joule-heating Effects and High Hydrophobicity-derived Anti-icing Properties. *J. Mater. Sci.* **2018**, *53*, 528−537.
(39) Olszowska, K.; Pang, J.; Wrobel, P. S.; Zhao, L.; Ta, H. Q.; Liu, Z.; Trzebicka, B.; Bachmatiuk, A.; Rummeli, M. H. Three-dimensional Nanostructured Graphene: Synthesis and Energy, Environmental and Biomedical Applications. *Synth. Met.* **2017**, *234*, 53−85.
(40) Ostomel, T. A.; Shi, Q.; Stoimenov, P. K.; Stucky, G. D. Metal Oxide Surface Charge Mediated Hemostasis. *Langmuir* **2007**, *23*, 11233−11238.
(41) Arnaud, F.; Tomori, T.; Carr, W.; McKeague, A.; Teranishi, K.; Prusaczyk, K.; McCarron, R. Exothermic Reaction in Zeolite Hemostatic Dressings: QuikClot ACS and ACS+®. *Ann. Biomed. Eng.* **2008**, *36*, 1708−1713.
(42) Chen, F.; Cao, X.; Yu, J.; Su, H.; Wei, S.; Hong, H.; Liu, C. Quaternary Ammonium Groups Modified Starch Microspheres for Instant Hemorrhage Control. *Colloids Surf., B* **2017**, *159*, 937−944.
(43) Li, H.; Cheng, W.; Liu, K.; Chen, L.; Huang, Y.; Wang, X.; Lv, Z.; He, J.; Li, C. Reinforced Collagen with Oxidized Microcrystalline Cellulose Shows Improved Hemostatic Effects. *Carbohydr. Polym.* **2017**, *165*, 30−38.
(44) Li, G.; Quan, K.; Xu, C.; Deng, B.; Wang, X. Synergy in Thrombin-Graphene Sponge for Improved Hemostatic Efficacy and Facile Utilization. *Colloids Surf., B* **2018**, *161*, 27−34.
(45) Probst, R. J.; Lim, J. M.; Bird, D. N.; Pole, G. L.; Sato, A. K.; Claybaugh, J. R. Gender Differences in the Blood Volume of Conscious Sprague-Dawley Rats. *J. Am. Assoc. Lab. Anim. Sci.* **2006**, *45* (2), 49−52.
(46) Sinert, R.; Guerrero, P.; Quintana, E.; Zehtabchi, S.; Kim, C.; Agbemadzo, A.; Baron, B. The Effect of Hypertension on the Response to Blood Loss in a Rodent Model. *Acad. Emerg. Med.* **2000**, *7* (4), 318−326.
(47) Page, A. Blood-injury Phobia. *Clin. Psycho. Rev.* **1994**, *14* (5), 443−461.
(48) Eryilmaz, M.; Ozer, T.; Menteş, O.; Torer, N.; Durusu, M.; Günal, A.; Uzar, A. I. Is the Zeolite Hemostatic Agent Beneficial in Reducing Blood Loss during Arterial Injury? *Turk. J. Trauma Emerg. Surg.* **2009**, *15*, 7−11.
(49) Martin, N. A.; Falder, S. A Review of the Evidence for Threshold of Burn Injury. *Burns* **2017**, *43*, 1624−1639.
(50) Power, G.; Moore, Z.; O'Connor, T. Measurement of pH, Exudate Composition and Temperature in Wound Healing: a Systematic Review. *J. Wound Care* **2017**, *26*, 381−397.
(51) Esechie, A.; Kiss, L.; Olah, G.; Horváth, E. M.; Hawkins, H.; Szabo, C.; Traber, D. L. Protective Effect of Hydrogen Sulfide in a Murine Model of Acute Lung Injury Induced by Combined Burn and Smoke Inhalation. *Clin. Sci.* **2008**, *115*, 91−97.
(52) Esechie, A.; Enkhbaatar, P.; Traber, D. L.; Jonkam, C.; Lange, M.; Hamahata, A.; Djukom, C.; Whorton, E. B.; Hawkins, H. K.; Traber, L. D.; Szabo, C. Beneficial Effect of a Hydrogen Sulphide Donor (sodium sulphide) in an Ovine Model of Burn-and Smoke-Induced Acute Lung Injury. *Br. J. Pharmacol.* **2009**, *158*, 1442−1453.
(53) Ahmad, A.; Szabo, C. Both the H2S Biosynthesis Inhibitor Aminooxyacetic Acid and the Mitochondrially Targeted H2S Donor AP39 Exert Protective Effects in a Mouse Model of Burn Injury. *Pharmacol. Res.* **2016**, *113*, 348−355.
(54) Souza, N. L. G.; Munk, M.; Brandão, H. M.; DeOliveira, L. F. C. Cytotoxicity and Compatibility of Polymeric Blend: Evaluation of the Cytotoxicity in Fibroblast Bovine Cells and Compatibility of Poly (ε-Caprolactone)/Poly (Methyl Methacrylate-co-Butyl Methacrylate) Blend Films. *Polym.-Plast. Technol. Eng.* **2017**, *56*, 1076−1083.
(55) Wan, Q.; Mao, L.; Liu, M.; Wang, K.; Zeng, G.; Xu, D.; Huang, H.; Zhang, X.; Wei, Y. Towards development of a Versatile and Efficient Strategy for Fabrication of GO Based Polymer Nano-composites. *Polym. Chem.* **2015**, *6*, 7211−7218.
(56) Tu, Y.; Lv, M.; Xiu, P.; Huynh, T.; Zhang, M.; Castelli, M.; Liu, Z.; Huang, Q.; Fan, C.; Fang, H.; Zhou, R. Destructive Extraction of Phospholipids from Escherichia coli Membranes by Graphene Nanosheets. *Nat. Nanotechnol.* **2013**, *8*, 594−601.
(57) Hu, W.; Peng, C.; Luo, W.; Lv, M.; Li, X.; Li, D.; Huang, Q.; Fan, C. Graphene-based Antibacterial Paper. *ACS Nano* **2010**, *4*, 4317−4323.

DOI: 10.1021/acsami.9b04956
ACS Appl. Mater. Interfaces XXXX, XXX, XXX−XXX